Mathematical Derivation, Circuits Design and Clinical Experiments of Measuring Blood Flow Volume (BFV) at Arteriovenous Fistula (AVF) of Hemodialysis (HD) Patients Using a Newly-Developed Photoplethysmography (PPG) Sensor

Paul C. P. Paul[1,3], Pei-Yu Chiang[1], D. C. Tarng[2], C. Y. Yang[2]
[1] Department of Electrical Engineering, National Chiao Tung University, Hsinchu 300, Taiwan
[2] Division of Nephrology in Taipei Veterans General Hospital, Taipei 112, Taiwan
[*] E-mail: pchao@mail.nctu.edu.tw

Abstract

Mathematical derivation of calculating blood flow volume (BFV) at arteriovenous fistula (AVF) using a newly-developed photoplethysmography (PPG) sensor is presented in this work. Also, the readout circuit of the PPG sensor intended to increase the signal-noise ratio (S/NR) is designed and presented in this work. The designed PPG sensor equipped with derived mathematical equations shows high correlation ($R^2 = 0.7563$) and low error (RMSE = 212 ml/min) as compared to the gold standard.

Keywords

Photoplethysmography (PPG) Sensor, Arteriovenous Fistula (AVF), Blood Flow Volume (BFV).

1. Introduction

Arteriovenous Fistula (AVF) refers to the surgically created junction between artery and vein at arm, which is the lifeline to patients suffering chronic kidney decease (CKD) and under hemodialysis (HD) treatment. In present clinical practice, the quality of AVF is accessed by measuring the blood flow volume (BFV) at a downstream spot to AVF, which is usually considered be at least 600 ml/min to maintain the least AVF quality for feasible HD treatment [1]. There are mainly two different instruments used to measure BFV near AVF, a noninvasive ultrasound Doppler machine and an invasive dilution concentration monitor. Both of them are too bulky to be used as portable devices for HD patients to collect continuous monitoring data for effective prognosis. This work is dedicated herein to develop a new portable photoplethysmography (PPG) sensor, computation algorithm and readout circuitry for measuring BFV at AVF.

PPG is an optical, noninvasive measurement method for sensing the intravascular changes of blood vessels. The merits of PPG sensors are small-sized, inexpensive and easy-to-use. Thus, they are widely used in various physiological information monitorings, such as for heart rate, blood pressure, blood oxygen saturation, respiration etc. There are some works published in the past on accessing AVF using a PPG sensor. Wu *et al.* [2][3] published their work on detecting degree of stenosis and arterial steal syndrome of AVF by applying a bilateral PPG sensor system. Different from multiple sensors employed by [2][3], Chiang *et al.* [4] designed a single PPG sensor to achieve BFV measurement at AVF. The resulted correlation coefficient R^2 of measured BFV data reaches 0.7. Chao *et al.* [5] published a work of approximating the BFV at AVF by neglecting the inertance term in the wave propagation model of pulsating blood vessels for solving the equations. However, some past works claimed that the effect of previously-ignored inertance on vessel wave propagation is more significant for HD patient than a normal person. Therefore, this work considers again the inertance in the wave propagation equation, and then solves the equations by a method, a Fourier series. With experiments and calibration conducted, a higher correlation coefficient R^2 of 0.7563 is resulted.

This works is organized as follow. In section 2, the mathematical derivation from PPG signals to average BFV at AVF is introduced. In section 3, the readout circuitry of the PPG sensors for clinical validation is proposed. In section 4, the clinical experiments and the experiment results are shown. Section 5 concludes the works with some inspiring discussion.

2. Theoretical Development

A typical PPG signal measured at AVF is shown in Fig. 1 and the coordinate system used in the mathematical derivation is shown in Fig. 2, where the blood vessel lies on z-axis and AVF is at $z = 0$.

2.1 Beer Lambert's Law

The origin of PPG can be described using the known physical theory, Beer Lambert's Law, which is as

$$PPG = I_0 R_{skin} e^{-\varepsilon_t c_t d_t} e^{-\varepsilon_b c_b d_b}, \quad (1)$$

where PPG indicates the PPG signals; I_0 indicates the intensity of the LED light source; R_{skin} indicates the reflectance coefficient of the skin; ε_t and ε_b indicate the absorption coefficients of tissues and blood respectively; c_t and c_b indicate the Mohr concentrations of tissues and blood respectively; d_t indicates the path length of light travelling through tissues; d_b indicates the path length of light travelling through blood, which is the diameter of the measured blood vessel. Moreover, consider blood oxygen saturation (SpO_2), the absorption coefficient and the concentration of blood can be expressed as [7]

$$\varepsilon_b c_b = \varepsilon_{HbO} \cdot SpO_2 + \varepsilon_{Hb} \cdot (1 - SpO_2) + \varepsilon_p \cdot c_p, \quad (2)$$

where ε_{HbO} and ε_{Hb} denotes the absorption coefficients of oxy-hemoglobin and hemoglobin respectively; SpO_2 denotes the blood oxygen saturation level; ε_p and c_p denote the absorption coefficient and Mohr concentration of plasma. Therefore, combining Eq. (1) and (2), the cross-sectional area of AVF, $A(t)$, can be described as

$$A(t) = f_1(PPG, SpO_2). \quad (3)$$

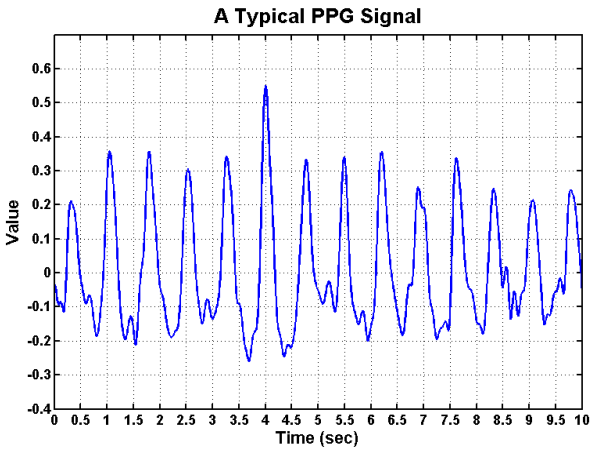

Fig. 1 A typical PPG signals measured at AVF.

Moreover, Eq. (3) can be expand to the cross-sectional area along z-axis as $A(z,t)$. For simplicity, the cross-sectional area is assumed to change linearly along *z-axis* at any time as

$$A(z,t)=\frac{A(L,t)-A(0,t)}{L}z+A(0,t), \tag{4}$$

where L denotes the length of the AVF. Hence, the cross-sectional area can be rewritten as

$$A(z,t)=f_2(z,PPG,SpO_2). \tag{5}$$

2.2 Linear Constitutive Equation

The linear constitutive equation between the cross-sectional area and the blood pressure can be written as

$$A(t)=A_0+C_0(p-p_0), \tag{6}$$

where C_0 is the compliance per unit length; A_0 is the cross-sectional area when blood pressure is equaled to p_0. Moreover, it is assumed that the systolic blood pressure (DBP) and diastolic blood pressure (SBP) happened at t=0 and t=t0 receptively. Therefore, Eq. (6) can be rewritten as

$$A(0)=A_{\max}=A_0+C_0(SBP-p_0), \tag{7}$$

$$A(t_0)=A_{\min}=A_0+C_0(DBP-p_0), \tag{8}$$

where SBP and DBP denote the systolic blood pressure (SBP) and the diastolic blood pressure (DBP) respectively; $A_{\max}$ and $A_{\min}$ denote the maximum and minimum cross-sectional area, which happened at systole (t=0) and diastole (t=t_0) respectively. Therefore, combining Eq. (7) and Eq. (8) yields

$$\frac{\partial p}{\partial A}=\frac{1}{C_0}=\frac{SBP-DBP}{A(0)-A(t_0)}=\frac{SBP-DBP}{A_{\min}-A_{\max}}. \tag{9}$$

2.4 Wave Propagation Model

To derived the relationship between blood pressure and blood flow volume (BFV), the wave propagation model provided by D. Bessems *et al.* [8] is introduced, which is as

$$\frac{\partial p}{\partial z}=-c_1\frac{8\pi\eta}{A^2}q-c_2\frac{\rho}{A}\frac{\partial q}{\partial t}, \tag{10}$$

where q denotes the instantaneous blood flow volume; η denotes the dynamic viscosity of blood; ρ denotes the blood density; c_1 and c_2 are as

$$c_1=\frac{\alpha^2}{\alpha^2-\sqrt{2}\alpha+1}\times\frac{\alpha^2}{4\sqrt{2}\alpha-4}, \tag{11}$$

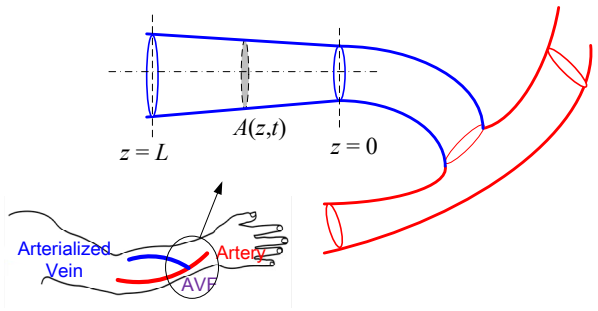

Fig. 2 The coordinate system of AVF used in the mathematical derivation.

$$c_2=\frac{\alpha^2}{\alpha^2-\sqrt{2}\alpha+1}, \tag{12}$$

where α denotes the Womersley number defined as

$$\alpha=r_0\sqrt{\frac{\omega\rho}{\eta}}, \tag{13}$$

where r_0 denotes the average radius of blood vessels; ω denotes the angular frequency of heart rate. Substituting Eq. (5) and (9) into the left side of Eq. (10) gives

$$\frac{SBP-DBP}{A_{\min}-A_{\max}}\frac{A(L,t)-A(0,t)}{L}=-c_1\frac{8\pi\eta}{A^2}q-c_2\frac{\rho}{A}\frac{\partial q}{\partial t}. \tag{14}$$

Furthermore, it is assumed that the pulsation of vein is so small that the cross-sectional area of vein, $A(L,t)$, can be viewed as a constant. Hence, Eq. (14) can be arranged to

$$\frac{SBP-DBP}{A_{\min}-A_{\max}}\frac{A_V-A(0,t)}{L}=-c_1\frac{8\pi\eta}{A^2}q-c_2\frac{\rho}{A}\frac{\partial q}{\partial t}, \tag{15}$$

where A_V denote the cross-sectional area of the vein.

2.5 Average Blood Flow Volume

To solve the average BFV from Eq. (15), frequency domain technique are introduced. The complex Fourier series of cross-sectional area are assumed to be as

$$A=\sum_{n=-\infty}^{\infty}a_n e^{j\omega nt}, \tag{16}$$

where j denotes the complex number $\sqrt{-1}$; a_n are the coefficients of each frequency components in complex form; ω is the angular frequency of heart rate. Similarly, the BFV can be expressed in complex Fourier series as

$$q=\sum_{n=-\infty}^{\infty}q_n e^{j\omega nt}. \tag{17}$$

Therefore, average BFV can be expressed as

$$\bar{q}=\frac{1}{T}\int_{t=0}^{T}q\,dt=\frac{1}{T}q_0, \tag{18}$$

where T is the period of heart rate. Substitution of Eq. (16) and Eq. (17) into Eq. (15) and focus on only non-time varying terms yields

$$K_1\sum_{(l+m+n=0)}a_l a_m a_n+K_2\sum_{(m+n=0)}a_m a_n=K_3 q_0+K_4\sum_n \Re\{a_{-n}q_n\}, \tag{19}$$

where $\Re\{\}$ denotes the real part of complex number; K_1 to K_4 is as

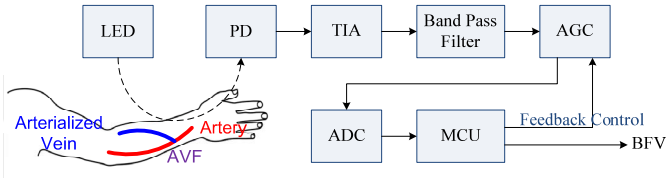

Fig. 3 The architecture of the designed readout circuit.

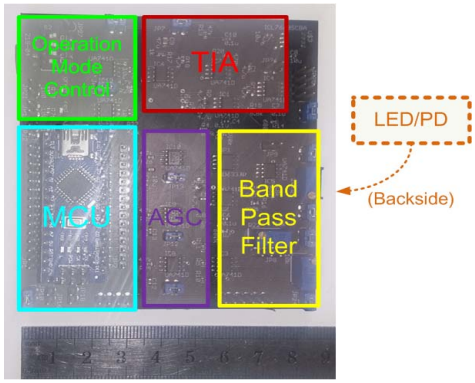

Fig. 4 The photo of the designed circuitries implementing on PCB.

$$K_1 = \frac{SBP - DBP}{A_{\min} - A_{\max}} \frac{A_v}{L}; \quad (20)$$

$$K_2 = -\frac{SBP - DBP}{A_{\min} - A_{\max}} \frac{1}{L}; \quad (21)$$

$$K_3 = -c_1 \pi \eta; \quad (22)$$

$$K_4 = 2c_2 \rho \omega. \quad (23)$$

Moreover, the approximation of the harmonic terms of BFV, q_n, are introduced from J. R. Womersley [9] as

$$q_n = f_3(K_1, K_2, a_0, a_n, \omega). \quad (24)$$

For simplicity, only the first two harmonic terms are considered. Substitution of Eq. (24) into Eq. (19) gives the equation of average BFV as

$$\bar{q} = f_4 \begin{pmatrix} T, SBP, DBP, PPG(0), PPG(t_0), SpO_2, \\ DC, \Re(i_1^{(1)}), \Im(i_1^{(1)}), \Re(i_2^{(1)}), \Im(i_2^{(1)}), \\ DC^2, \Re(i_1^{(2)}), \Im(i_1^{(2)}), \Re(i_2^{(2)}), \Im(i_2^{(2)}), \end{pmatrix}, \quad (25)$$

where $\Im\{\}$ denotes the real imaginary of complex number; DC denotes the direct component of PPG signals; $i_n^{(k)}$ denotes the n-th harmonic term of the k-th power of PPG signals as

$$PPG^k(t) = \sum_{n=-\infty}^{\infty} i_n^{(k)} e^{jn\omega t}. \quad (26)$$

3. Circuit Design

The circuit architecture of the designed PPG circuitries are shown in Fig. 3, and the photo of the proposed readout circuits implemented on PCB are shown in Fig. 4.

3.1 Transimpedence Amplifier (TIA)

It is known that the output signals of the photodiode are current signals. However, voltage signals are much preferred in discrete circuit. Therefore, a transimpedence amplifier (TIA) is added to transform the current signals to voltage signals. The proposed TIA circuitries and the photodiode are shown in Fig. 5. The PD is designed to be operated under zero biased mode, which claims the advantage of high linearity.

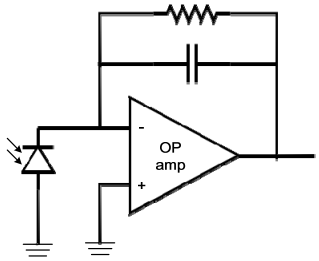

Fig. 5 The proposed transimpedence amplifier (TIA).

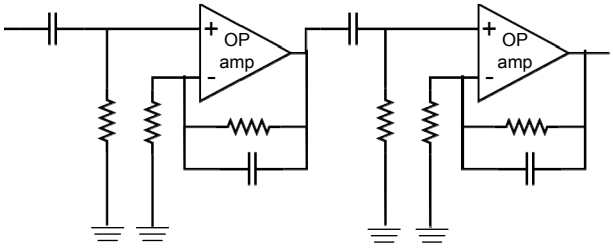

Fig. 6 The proposed band pass filter.

3.2 Band-Pass Filter

A fourth order band pass filter, as shown in Fig. 6, is proposed in the circuitries to filter out the noise in raw signals. It is known that the dominant frequency of PPG signals is heart beat frequency (about 0.8-2 Hz), and the harmonic terms of PPG signals are needed for calculating BFV. Therefore, in this work, the cutoff frequency of the proposed filter is designed to be 0.5 Hz and 10 Hz.

3.3 Auto Gain Control (AGC)

In order to increase the signal-noise ratio (S/NR), an auto gain control (AGC) circuitries are proposed in this work by fully using the dynamic range of the analog-digital converter (ADC). The auto gain control circuitries are composed of a programmable gain amplifier (PGA) feedback controlled by micro-controller unit (MCU). Also, the AGC circuitries can be used to prevent signal saturation by decrease the gain of the PGA.

4. Clinical Experiment

There are total 27 patients participating the experiments and the basic physiological information of the volunteers is shown in Table I. The gold standard instrument used in the experiment is the invasive dilution concentration sensor. After neural network calibration, the correlation plot of the measurement result is shown in Fig. 7 and the Bland-Altman plot is shown in Fig. 8, where the correlation coefficient R^2 is about 0.7563 and the root mean square error is about 212 ml/min.

Table. I The basic physiology information of patients

Term	Mean (± SD)
Age	68.79 (± 14.20) years
Male (Female)	11 (16)
Heart rate	85.44 (± 17.83) bpm
SBP	148.48 (± 21.30) mmHg
DBP	73.55 (± 15.75) mmHg
SpO_2	98.28 (± 1.58) %
Height	159.73 (± 8.56) cm
Weight	63.63 (± 9.26) kg

5. Conclusion

A mathematical derivation on the equations prescribing wave propagation of blood vessels for calculating the blood flow volume (BFV) at arteriovenous fistula (AVF) is successfully completed in this work by solving the differential equation in frequency domain in Fourier series. PPG sensor and readout circuits are designed and realized to increase the quality of acquired PPG signal for better validation on the equations. Finally, the clinical experiment shows a good correlation (R^2 = 0.7563) and limited error (RMSE = 212 ml/min) associated with 95% confidence level, which is adequate for ensuring AVF quality in clinic practice.

6. Acknowledgment

The authors appreciate the supports from Ministry of Science and Technology of Taiwan, R.O.C. under the grant no. MOST 105-2634-F-009-002, 105-2923-M-009-006, 106-3114- E-009-004, NARL-IOT-105-006, and it was also supported in part by the Novel Bioengineering and Technological Approaches to Solve Two Major Health Problems in Taiwan sponsored by the Taiwan Ministry of Science and Technology Academic Excellence Program under Grant Number: MOST 106-2633-B-009-001.

7. References

[1] National Kidney Foundation. “KDOQI Clinical Practice Guidelines and Clinical Practice Recommendations for 2006 Updates: Hemodialysis Adequacy, Peritoneal Dialysis Adequacy and Vascular Access.” *Am J Kidney Dis*, 48:S1-S322, 2006 (suppl 1).

[2] J.-X. Wu, C.-H. Lin, M.-J. Wu, C.-M. Li, B.-Y. Lim and Y.-C. Du, "Bilateral photoplethysmography analysis for arteriovenous fistula dysfunction screening with fractional-order feature and cooperative game-based embedded detector", *Healthc Technol Lett*, Jun, 2(3), pp. 64– 69, 2015.

[3] J.‐ X. Wu, G.‐ C. Chen, M.‐ J. Wu, C.‐ H. Lin, T. Chen, "Bilateral photoplethysmography for arterial steal detection in arteriovenous fistula using a fractional-order decision-making quantizer", *Med Biol Eng Comput*, pp. 55:257–270, 2017.

[4] P. Y. Chiang, P. C. P. Chao, D. C. Tarng and C. Y. Yang, "A Novel Wireless Photoplethysmography Blood Flow Volume Sensor for Assessing Arteriovenous Fistula of Hemodialysis Patients," *IEEE Transactions on Industrial Electronics*, vol. PP, no. 99, pp. 1-1, 2017.

[5] P. C. P. Chao and P. Y. Chiang, "Theoretical development with proper approximation and the corresponding clinical experiments for PPG sensor monitoring blood flow volume of hemodialysis patients with arteriovenous fistula," *2017 International Conference on Applied System Innovation (ICASI)*, Sapporo, pp. 311-314, 2017.

[6] W. Huberts, A.S. Bode, W. Kroon, R.N. Planken, J.H.M. Tordoir, F.N. van de Vosse, E.M.H. Bosboom, "A pulse wave propagation model to support decision-making in vascular access planning in the clinic", Medical Engineering & Physics, Volume 34, Issue 2, pp. 233-248, ISSN 1350-4533, 2012.

[7] M. Nitzan, A. Romem and R. Koppel, "Pulse oximetry: fundamentals and technology update", *Medical Devices (Auckland, N.Z.)*, pp. 231–239, 2014.

[8] D. Bessems, M. Rutten and F. V. D. Vosse, "A wave propagation model of blood flow in large vessels using an approximate velocity profile function", *Journal of Fluid Mechanics*, Volume 580 10 June , pp. 145-168, 2007.

[9] J. R. Womersley, "Method for the calculation of velocity, rate of flow and viscous drag in arteries when the pressure gradient is known", *The Journal of Physiology*, pp.(3):553-563, 1955.

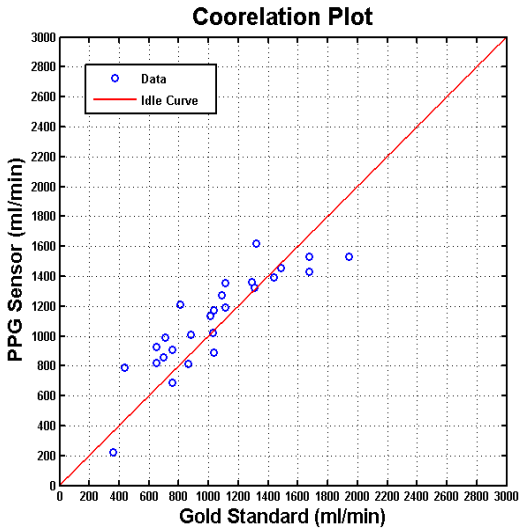

Fig. 7 The correlation plot of the experiment results

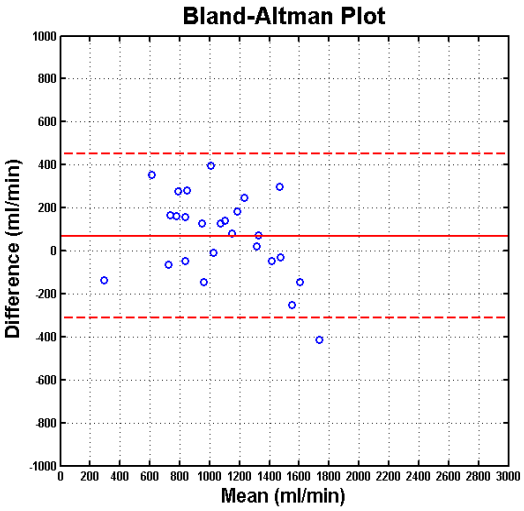

Fig. 8 The Bland-Altman plot of the experiment results